Atmos. Chem. Phys. Discuss., 9, 2791–2822, 2009
www.atmos-chem-phys-discuss.net/9/2791/2009/

Atmospheric Chemistry and Physics Discussions

This discussion paper is/has been under review for the journal *Atmospheric Chemistry and Physics (ACP)*. Please refer to the corresponding final paper in *ACP* if available.

Inferring ozone production in an urban atmosphere using measurements of peroxynitric acid

K. M. Spencer[1], D. C. McCabe[2,*], J. D. Crounse[1], J. R. Olson[3], J. H. Crawford[3], A. J. Weinheimer[4], D. J. Knapp[4], D. D. Montzka[4], C. A. Cantrell[4], R. S. Anderson[4], R. L. Mauldin III[4], and P. O. Wennberg[2,5]

[1]Division of Chemistry and Chemical Engineering, California Institute of Technology, Pasadena, CA, USA
[2]Division of Geological and Planetary Sciences, California Institute of Technology, Pasadena, CA, USA
[3]NASA Langley Research Center, Hampton, VA, USA

[4] National Center for Atmospheric Research, Boulder, CO, USA
[5] Division of Engineering and Applied Science, California Institute of Technology, Pasadena, CA, USA
[*] now at: AAAS Science & Technology Policy Fellow, United States Environmental Protection Agency, Washington, DC, USA

Received: 1 December 2008 – Accepted: 15 December 2008 – Published: 28 January 2009

Correspondence to: K. M. Spencer (kspencer@caltech.edu)

Published by Copernicus Publications on behalf of the European Geosciences Union.

Abstract

Observations of peroxynitric acid (HO_2NO_2) obtained simultaneously with those of NO and NO_2 provide a sensitive measure of the ozone photochemical production rate. We illustrate this technique for constraining the ozone production rate with observations obtained from the NCAR C-130 aircraft platform during the Megacity Initiative: Local and Global Research Observations (MILAGRO) intensive in Mexico during the spring of 2006. Sensitive and selective measurements of HO_2NO_2 were made in situ using chemical ionization mass spectrometry (CIMS). Observations were compared to modeled HO_2NO_2 concentrations obtained from the NASA Langley highly-constrained photochemical time-dependent box model. The median observed-to-calculated ratio of HO_2NO_2 is 1.18. At NO_x levels greater than 15 ppbv, the photochemical box model underpredicts observations with an observed-to-calculated ratio of HO_2NO_2 of 1.57. As a result, we find that at high NO_x, the ozone production rate calculated using measured HO_2NO_2 is faster than predicted using accepted photochemistry. Inclusion of an additional HO_x source from the reaction of excited state NO_2 with H_2O or reduction in the rate constant of the reaction of OH with NO_2 improves the agreement.

1 Introduction

Peroxynitric acid, HO_2NO_2, is an important reservoir of both HO_x (HO_x=OH+HO_2) and NO_x (NO_x=NO+NO_2) radicals. These radicals are of primary atmospheric importance as they influence the production and degradation of tropospheric ozone and numerous volatile organic compounds (Murphy et al., 2004). Ozone production in urban environments is initiated by OH radicals and requires sunlight, NO_x, and hydrocarbons. The relative amounts of these species control the rate of ozone production (Seinfeld and Pandis, 2006).

The only known pathway for the formation of HO_2NO_2 in the atmosphere is the association reaction of HO_2 and NO_2, R1 (Niki et al., 1977). HO_2NO_2 is lost via thermal

decomposition, R-1 (Graham et al., 1977, 1978; Zabel et al., 1995; Gierczak et al., 2005); UV and visible/near-IR photolysis, R2 (Macleod et al., 1988; Roehl et al., 2002; Knight et al., 2002); and reaction with the OH radical, R3 (Trevor et al., 1982; Smith et al., 1984; Barnes et al., 1986; Jimenez et al., 2004).

$$HO_2 + NO_2 + M \rightleftharpoons HO_2NO_2 + M \quad \text{(R1)}$$

$$HO_2NO_2 + h\nu \rightarrow \text{products} \quad \text{(R2)}$$

$$HO_2NO_2 + OH \rightarrow H_2O + NO_2 + O_2 \quad \text{(R3)}$$

The relative importance of the HO_2NO_2 sinks depends on temperature, pressure, OH radical concentration, and the UV/IR radiation field. The lifetime of HO_2NO_2 with respect to thermal decomposition varies due to the strong temperature dependence of this process (Kim et al., 2007). As temperature decreases, loss due to photolysis and reaction with OH radical become increasingly important. At altitudes greater than 7 km, photolysis and reaction with OH become the dominant loss mechanisms (Roehl et al., 2002). The formation of HO_2NO_2 followed by its loss via reaction with OH forms a NO_x-catalyzed sink of HO_x radicals (Roehl et al., 2002).

The role of HO_2NO_2 in photochemistry of the lower troposphere has been less explored, in part because of a paucity of observations of this compound. In situ measurements of HO_2NO_2 have been obtained previously in the free troposphere during the 2004 INTEX-NA campaign (Kim et al., 2007) and in Antarctica (Slusher et al., 2001). An indirect estimate of the HO_2NO_2 abundance was obtained from the sum of peroxynitrate observations during the 2000 TOPSE campaign (Murphy et al., 2004).

Here, we present in situ measurements of HO_2NO_2 in and around Mexico City. These measurements were made in March of 2006 from the NCAR C-130 aircraft platform during the MILAGRO field experiment. One goal of the MILAGRO mission, and the focus of the C-130 flights, was to investigate the processing and outflow of pollution from Mexico City. Most flights occurred during the daytime hours at altitudes below 7 km and temperatures between 250 and 300 K. This study is limited to six of the

MILAGRO flights (8, 22, 23, 26, 28, and 29 March) during which all necessary species were measured. A photochemical steady-state approximation of HO_2NO_2 under MILAGRO conditions is discussed, and measured HO_2NO_2 concentrations are compared to those predicted by the NASA Langley Research Center LaRC highly-constrained photochemical time-dependent box model (NASA LaRC box model). A simplified method of estimating the rate of ozone production using HO_2NO_2 is compared to full NASA LaRC box model calculations of the rate of ozone production.

2 Method

2.1 Instrumentation

NO and NO_2 mixing ratios were measured by photofragmentation/chemiluminescence. The overall uncertainty for these measurements is 10–20% (Campos et al., 1998; Weinheimer et al., 1998). HO_2 mixing ratios were determined by chemical-conversion/chemical ionization mass spectroscopy with an uncertainty of 35% (Cantrell et al., 2003). H_2O mixing ratios were measured using a dew/frost point water hygrometer.

HO_2NO_2 measurements were made using the Caltech chemical ionization mass spectrometry (CIMS) instrument. The instrument has been described in detail previously by Crounse et al. (2006). Briefly, the Caltech CIMS consists of a flow tube controlled at 35 mbar total pressure where a reagent ion, CF_3O^-, interacts with ambient air diluted 1:4 with dry nitrogen. Ions are sampled from the flow tube into a quadrupole mass filter and detected with a channel electron multipler. Each mass-to-charge ratio is observed for ∼0.5 s. HO_2NO_2 masses were monitored every ∼15 s.

Negative ion chemistry of CF_3O^- has been shown to provide sensitive and selective detection of many inorganic and organic acids (Huey et al., 1996; Amelynck et al., 2000a,b; Crounse et al., 2006) and was exploited in this work to detect HO_2NO_2. The reaction of CF_3O^- with acids follows several pathways. Reaction with strong acids

proceeds via fluoride ion transfer (Huey et al., 1996) while reaction with weaker acids yields clusters of reagent ion and analyte (Amelynck et al., 2000a). HO_2NO_2 reacts with CF_3O^- via fluoride ion transfer (R4), clustering (R5) (Crounse et al., 2006), and a HF elimination Reaction (R6), providing three distinct ion signals. Reactions (4–6) are complicated by competing reactions with CF_3O^- water cluster ($CF_3O^- \cdot H_2O$).

$$CF_3O^- + HO_2NO_2 \rightarrow HF \cdot OONO_2^- \ (m/z\ 98) + CF_2O \quad \text{(R4)}$$

$$CF_3O^- + HO_2NO_2 \rightarrow CF_3O^- \cdot HO_2NO_2 (m/z\ 164) \quad \text{(R5)}$$

$$CF_3O^- + HO_2NO_2 \rightarrow CF_2O \cdot OONO_2^- (m/z\ 144) + HF \quad \text{(R6)}$$

2.1.1 Sensitivity and calibration

Due to differences in reactivity of CF_3O^- and its water cluster, the sensitivity of the CIMS instrument to the ion products of the three channels (R4, R5, R6) is dependent on the mixing ratio of water vapor in the flow tube (Crounse et al., 2006). This dependence is quantified via laboratory measurements. A small quantity of HO_2NO_2 was introduced into the flow tube. The flow tube humidity was controlled using mass flow controllers to adjust the ratio of air saturated with water vapor to dry zero air. Humidity was quantified by Fourier Transform Infrared (FTIR) spectroscopy using HITRAN line lists (Rothman et al., 2005) and the commercial spectral manipulation software package GRAMS (Galactic Industries Inc.). The sensitivity of the instrument to the fluoride ion transfer and cluster channels of HO_2NO_2 as a function of H_2O mixing ratio in the flow tube was determined and is presented in Fig. 1. Sensitivity is expressed in ion counts, normalized by the ion counts of the +1 isotopes of the reagent ions, $^{13}CF_3O^-$ and $^{13}CF_3O^- \cdot H_2O$, per pptv of HO_2NO_2. The yield of R6 is typically one-third that of R5. Due to the low reaction yield, R6 is not used to quantify the ambient observations of HO_2NO_2.

During calibration, the concentration of HO_2NO_2 in the flow tube was determined by thermally decomposing the HO_2NO_2 into NO_2 (R-1) and quantifying the resultant NO_2

using CIMS with SF_6^- as the reagent ion (R7) (Huey et al., 1995):

$$SF_6^- + NO_2 \rightarrow SF_6 + NO_2^- \ (m/z\ 46) \quad \text{(R7)}$$

NO_2 is not detected with high sensitivity using CF_3O^-.

Synthesis of HO_2NO_2 was performed offline using the procedure described in Roehl et al. (2002); gas-phase HO_2NO_2 was produced by flowing dry N_2 over the solution of HO_2NO_2. A small portion of this flow was directed through a critical orifice into a PTFE three-way valve which directed the flow through either a heated or unheated glass inlet tube (6 mm OD). The heated inlet tube was kept at 190°C, a temperature at which 99.8% of the HO_2NO_2 decomposed, as determined by monitoring the signal with CF_3O^- at *m/z* 98. The unheated inlet was maintained at room temperature. The sensitivity of the CIMS to NO_2 was determined using a dilute mixture of NO_2 in N_2; the concentration of NO_2 in this mixture was quantified with FTIR using HITRAN line lists (Rothman et al., 2005) and the commercial spectral manipulation software package GRAMS (Galactic Industries Inc.).

The CIMS sensitivity to HO_2NO_2 was determined by back-to-back measurements of the products of R4, R5, and R7. HO_2NO_2 was added through the room temperature inlet and measured using CF_3O^- as the reagent ion. Next, HO_2NO_2 was added through the heated inlet and NO_2 was measured using SF_6^- as the reagent ion (R7). Background NO_2 from NO_2 impurity in the HO_2NO_2 solution was measured using SF_6^- by passing the HO_2NO_2 through the room temperature inlet; this background signal was subtracted from the NO_2 signal when the heated inlet was used. The signals from R4 and R5 obtained using the room temperature inlet were also corrected for the small amount of HO_2NO_2 that did not dissociate in the heated inlet and other backgrounds (see below) by monitoring those masses using CF_3O^- as the reagent ion with the heated inlet in use. This procedure was repeated at a number of humidities to obtain water-dependent calibration functions for each ion product. Post-mission laboratory calibrations for HO_2NO_2 were conducted. During flight, isotopically labeled HNO_3 was periodically added to the flow tube to monitor the stability of the instrument sensitivity. Sensitivity of the instrument to HNO_3 was consistent and comparable during flight and laboratory calibrations indicating the sensitivity of the instrument to HO_2NO_2 was consistent.

In the absence of HO_2NO_2, ion signals at *m/z* 98 and *m/z* 164 are non-zero, and these background signals must be accounted for in the data analysis. These background signals were measured during flight by periodically passing ambient air through a filter consisting of alumina pellets coated with palladium and nylon wool coated with sodium bicarbonate, quantitatively removing HO_2NO_2. This technique is described in Crounse et al. (2006).

2.1.2 Ambient HO_2NO_2 concentration

HO_2NO_2 concentrations are calculated from the signals observed at *m/z* 98 and *m/z* 164 after normalization by the amount of reagent ion signal, subtraction of background signals, and application of the appropriate sensitivity factor for HO_2NO_2.

Acetate in the form $HF \cdot CH_3C(O)O^- \cdot H_2O$ is a known interference in the *m/z* 98 signal. $HF \cdot CH_3C(O)O^- \cdot H_2O$ is seen at *m/z* 97, with approximately 2.5% of the *m/z* 97 signal appearing at *m/z* 98 due to heavy isotopes of the ion. Because the *m/z* 97 signal was not monitored during these flights, the interference at *m/z* 98 was estimated from the monitored signal of the acetate-fluoride transfer ion ($HF \cdot CH_3C(O)O^-$) at *m/z* 79 and ambient water levels, using a function derived through post-mission laboratory measurements. There are no interferences of which we are aware at *m/z* 164. Background signals were measured (as described above) about every 15 min and are used to model background levels during the flight.

A scatter plot of the independent determinations of HO_2NO_2 calculated from the *m/z* 98 and the *m/z* 164 signals is shown in Fig. 2. During the flight, there is an ~8 s delay between a *m/z* 98 measurement and the corresponding *m/z* 164 measurement. Only observations obtained when the measured NO_y differs by less than 10% between *m/z* 98 and *m/z* 164 sampling times are included in Fig. 2. The slope of the robust fit line (DuMouchel and O'Brien, 1989; Street et al., 1988) is 0.90; intercept is 0.76 pptv;

R^2=0.94. These independent measurements are in good agreement, providing confidence in the use of this ion chemistry to quantify HO_2NO_2.

The concentration of HO_2NO_2 used in the subsequent analysis is determined by combining the independent measurements from *m/z* 98 and *m/z* 164 as follows. When the water mixing ratio in the flow tube is less than or equal to 200 ppmv, the *m/z* 98 measurement is used because the sensitivity at *m/z* 164 is low (Fig. 1; recall that the ambient air pulled into the flow tube is diluted 1:4 with dry N_2). When the water mixing ratio in the flow tube is between 200 to 500 ppmv, the mean of the m/z 98 and the *m/z* 164 measurements is used. At water vapor mixing ratios greater than 500 ppmv, the *m/z* 164 measurement is used exclusively. Although the sensitivity is somewhat lower at *m/z* 164 than at *m/z* 98 for water mixing ratios between 500 to 1000 ppmv, higher backgrounds and interference from acetate at *m/z* 98 make the cluster ion (*m/z* 164) a more robust measure of HO_2NO_2 than the fluoride transfer product ion (*m/z* 98) at these higher water mixing ratios.

The uncertainty in the PNA measurements is approximately (30% + 30 pptv). The uncertainty reflects the sum of the precision of the data determined by the counting statistics of the ions, the variability of the background signal, and the uncertainty of the sensitivities shown in Fig. 1.

2.2 Photochemical time-dependent box model

Calculated concentrations of HO_2, NO_2, and HO_2NO_2 and rates of ozone production were obtained from a highly-constrained photochemical time-dependent box model (NASA LaRC box model) (Olson et al., 2006). The modeling approach used is based on the assumption of a diurnal equilibrium (Olson et al., 2006, 2004; Frost et al., 2002; Jaegle, 2000). Model inputs include observations of atmospheric parameters such as temperature, pressure, water vapor, and critical long-lived chemical precursor species (O_3, CO, NO, CH_4, non-methane hydrocarbons (NMHC), acetone). With the exception of NO and the radiation field, the atmospheric state is held

constant throughout the model run. NO varies diurnally; however reactive nitrogen, NO_y=NO+NO_2+NO_3+2N_2O_5+HONO+HO_2NO_2, is held constant with partitioning as determined by the model. The amount of total reactive nitrogen is determined so that NO matches the observed value at the time of the measurement. Additional constraints are implemented if data are available. These additional constraints include methanol, ethanol, H_2O_2, CH_3OOH, HNO_3, PAN, acetic acid, and formic acid. Concentrations of these species are computed by the model when data are unavailable.

The model chemistry includes HO_x–NO_x–CH_4 gas phase reactions based on the recommendations of Atkinson et al. (2004) and Sander et al. (2003). In addition, the model uses the rate for $O(^1D)$ quenching by N_2 suggested by Ravishankara et al. (2002), temperature dependent quantum yields for acetone photolysis from Arnold et al. (2005), and the parameterization for near-IR photolysis of HO_2NO_2 described by Roehl et al. (2002). Nonmethane hydrocarbon chemistry is based on the condensed mechanism of Lurmann et al. (1986) with modifications included to address remote low-NO_x conditions. Explicit chemistry is included for C_2H_6, C_3H_8, C_2H_4, isoprene, and benzene. C_4 and higher alkanes are lumped together, as are C_3 and higher alkenes, and aromatics other than benzene. Photolysis rate coefficients are based on spectroradiometer measurements (Shetter and Muller, 1999). The diurnal profiles of the photolysis rates are computed by a DISORT four-stream implementation of the Tropospheric Ultraviolet Visible (TUV) radiative transfer code (Madronich and Flocke, 1998). These calculated profiles are then normalized to match the instantaneous observations at the time of measurement.

Model calculations use the 1-min merged data set available on the INTEX-B public data archive (http://www-air.larc.nasa.gov). In this study, we limit the analysis to those points that include direct measurement of NMHCs.

2.3 Photochemical steady-state

At photochemical steady state, production and loss of HO_2NO_2 are equal and R1–R3 yield (Kim et al., 2007):

$$[HO_2NO_2]_{ss} = \frac{k_1[HO_2][NO_2]}{J_2 + k_{-1} + k_3[OH]} \quad (1)$$

For the conditions experienced during the MILAGRO flights, the lifetime of HO_2NO_2 with respect to thermal decomposition was less than one hour while the lifetimes with respect to UV/IR photolysis and reaction with OH were on the order of 1 day and 6 days, respectively. Under these conditions, the steady-state concentration of HO_2NO_2 simplifies to:

$$[HO_2NO_2]_{ss} \approx \frac{k_1[HO_2][NO_2]}{k_{-1}} \quad (2)$$

To evaluate whether the simplified assumption for steady state (Eq. 2) is robust for MILAGRO conditions, NASA LaRC box model predictions of HO_2 and NO_2 were used in the right-hand side of Eq. (2) to calculate HO_2NO_2 using the steady state assumption ($[HO_2NO_2]_{ss}$). $[HO_2NO_2]_{ss}$ was then compared to the full diurnal equilibrium model predictions of HO_2NO_2 (shown in Fig. 3). The slope of the robust fit line (DuMouchel and O'Brien, 1989; Street et al., 1988) is 1.02 and the intercept is 0.10 pptv. R^2=0.99.

The HO_2 mixing ratio measurements measured from the C-130 were not sufficiently precise to provide for a direct comparison between the measurements of HO_2NO_2 and the steady state calculation of $[HO_2NO_2]_{ss}$ using observed HO_2 and NO_2. However, the mean observed concentration of HO_2 was within 15% of the mean concentration of the NASA LaRC box model estimate for each of the flights used in this analysis.

3 Comparisons with NASA LaRC photochemical box model

An example time trace for HO_2NO_2 is illustrated in Fig. 4. During this flight (29 March 2006), the C-130 flew in and out of air masses heavily impacted by pollution from Mexico City. Variations in the measured and modeled HO_2NO_2 mixing ratio closely follow variations in NO_2.

Observed HO_2NO_2 mixing ratios, colored by NO_x mixing ratios, are compared to the NASA LaRC box model calculation of HO_2NO_2 mixing ratios in Fig. 5. The slope of the robust fit line is 0.81 and the intercept is 6.74 pptv. Although overall agreement is good (R^2=0.82), there is a tendency for the model to underpredict HO_2NO_2 concentrations at NO_x levels greater than 15 ppbv (shown by the red and orange colors in Fig. 5). Underprediction of HO_2NO_2 at elevated NO_x levels is in agreement with previous findings of Murphy et al. (2004) and Kim et al. (2007).

4 Ozone production

Photochemical ozone production is the result of oxidation of CO and hydrocarbons in reactions involving NO_x and HO_x. This process is regulated by the partitioning of species within these chemical families (Seinfeld and Pandis, 2006). The rate of ozone production can be calculated using Eq. (3) (Jacob, 1999).

$$P_{O_3} = k_{RO_2+NO}[RO_2][NO] + k_{HO_2+NO}[HO_2][NO] \quad (3)$$

The rate constants for the reactions of peroxyradicals (including HO_2) with NO are similar, so P_{O_3} can be approximated as:

$$P_{O_3} \approx k_{HO_2+NO}[NO]([RO_2] + [HO_2]) \quad (4)$$

In polluted atmospheres, HO_2 is produced primarily from the reaction of RO_2 with NO and therefore, the sum of all non-HO_2 peroxy radicals will be closely and linearly related to the concentration of HO_2 (e.g., Jacob, 1999).

$$P_{O_3} = Zk_{HO_2+NO}[HO_2][NO] \quad (5)$$

where Z is a number generally close to 2 in polluted air. With $K_{eq}=k_1/k_{-1}$, solving Eq. (2) for $[HO_2]$ and substituting into Eq. (5) yields:

$$P_{O_3}=\frac{Zk_{HO_2+NO}[HO_2NO_2][NO]}{K_{eq}[NO_2]} \quad (6)$$

In Fig. 6, we plot P_{O3} from the NASA LaRC box model versus $k_{HO_2+NO}[HO_2NO_2][NO]/K_{eq}[NO_2]$ to estimate Z. Using the NASA LaRC box model, we examined the predictions of Eq. (6). We limit this analysis to times when the solar zenith angle is < 80°. The slope of the polyfit fit line, Z, in Fig. 6 is 1.77. The correlation is high (R^2=0.99) suggesting that the production of ozone under MILAGRO conditions can be estimated directly from Eq. (6) using measured HO_2NO_2, NO, and NO_2 with Z=1.77. Figure 7 (top panel) shows the rate of ozone production along the flight track as calculated using observed values of HO_2NO_2, NO, and NO_2 in Eq. (6) compared to the rate of ozone production predicted by the NASA LaRC box model (bottom panel).

5 Discussion and conclusions

Because of the high correlation of RO_2 and HO_2 in urban air, HO_2NO_2 concentrations provide a proxy for the concentration of peroxy radicals and thus for the ozone production rate. In a polluted atmosphere, efficient HO_x chain propagation occurs during oxidation of hydrocarbons in which a hydrogen atom is attached to the alkoxy carbon. Hydrocarbons are oxidized by OH to form peroxy radicals. The peroxy radicals readily react with NO to produce alkoxy radicals and NO_2 and thus ozone. Alkoxy radicals combine with O_2 to form carbonyl compounds and HO_2 radicals, which subsequently react with NO to form OH and NO_2. When all HO_2 originates from RO_2, Z in Eq. (6) is 2. Because other sources of HO_2 exist, e.g., photolysis or reaction with OH of tertiary aldehydes and CH_2O (Jacob, 1999), the value is somewhat smaller, 1.77.

The rate of ozone production is sensitive to the rate of HO_x production and the amount of NO_x present. At a fixed HO_x production rate, the rate of ozone production increases with NO_x until NO_x reaches a level where the rate of nitric acid formation via R8 reduces HO_x levels and photochemistry slows.

$$OH + NO_2 + M \rightarrow HNO_3 + M \quad (R8)$$

This behavior can be seen in the model chemistry (Fig. 8, right panel). Ozone production rates for these MILAGRO flights calculated by the NASA LaRC box model are plotted versus NO levels and colored by the mixing ratio of CH_2O. CH_2O is used here as a proxy for the HO_x production rate (Seinfeld and Pandis, 2006). At low NO, the ozone production rate increases with NO at a fixed level of CH_2O, i.e., NO_x-limited behavior. At high NO, the ozone production rate becomes independent of or even decreases with NO at a fixed level of CH_2O, i.e., NO_x-saturated behavior.

In contrast to NASA LaRC box model calculations, the rate of ozone production estimated from observed HO_2NO_2, NO, and NO_2 does not show a saturation behavior (Fig. 8, left panel). At high NO, observed HO_2NO_2 levels continue to increase with NO, in contrast to model predictions. This suggests that the NASA LaRC box model underestimates the HO_2 levels and therefore either the HO_x production/loss rate is under/over estimated at elevated NO levels. This is consistent with observed HO_2NO_2 mixing ratios greater than NASA LaRC model predictions at NO_x levels greater than 15 ppbv shown in Fig. 5.

Observed values of HO_2NO_2, and hence HO_2, greater than those predicted by the NASA LaRC box model are consistent with a number of urban measurements of HO_2. Several recent studies have pointed to possible missing HO_x sources in urban air. At high NO_x concentrations, HO_2 levels calculated using highly constrained box models were significantly less than measured HO_2 levels during summertime in Nashville, Birmingham, and New York City (Martinez et al., 2003; Heard et al., 2004; Emmerson et al., 2005; Ren et al., 2003) and in New York City and Tokyo in the winter (Ren et al., 2006; Kanaya et al., 2007). Martinez et al. (2003) reported daytime HO_2 levels 1.56 times modeled values in Nashville in 1999. The difference between measured and modeled HO_2 was positively correlated with high NO_x mixing ratios. In Birmingham,

England in the summer of 1999 and winter of 2000, Heard et al. (2004) observed HO_2 levels 1.78 and 2.04 times modeled values, respectively. They found that the observed HO_2 concentrations were particularly insensitive to changes in NO_x levels. Summertime levels of HO_2 in New York City in 2001 were underestimated, with observed levels 1.24 times modeled values. The difference between measured and calculated HO_2 depended on the time of day. At midday, the observed and modeled values were found to agree very well while the model tended to underestimate the observations when NO_x was high, usually during the morning hours (Ren et al., 2003). Similar results where found in Tokyo during the winter of 2004. Daytime HO_2 concentrations were underestimated, with observed HO_2 levels 2.08 times modeled values. These comparisons were sensitive to the assumed hydrocarbon levels. When the concentrations of alkenes and reactive alkanes used in the model were increased by factors of 3 and 5, respectively, the observed-to-modeled HO_2 ratio decreased to 1.13. Continued underestimation of HO_2 concentrations occurred at high NO_x mixing ratios (Kanaya et al., 2007). The higher than expected levels of HO_2 suggest higher rates of ozone production than can be accounted for using known chemistry.

Not all studies have found excess HO_2. Indeed, several studies have found overpredictions of HO_2 levels by photochemical box models even at high NO_x concentrations. HO_2 concentrations were overestimated in the Los Angeles basin, Mexico City, and summertime Tokyo (George et al., 1999; Shirley et al., 2006; Kanaya et al., 2007). George et al. (1999) reported daytime HO_2 levels 0.67 times calculated values downwind of Los Angeles in 1993. The agreement for observed and calculated HO_2 was quite good in the early morning hours, but calculated HO_2 concentrations were found to be significantly higher than observations during midday. In Mexico City in 2003, Shirley et al. (2006) determined that observations of HO_2 were 0.79 times calculated values of HO_2 during the midday. However, they also calculated an observed-to-modeled ratio of 1.17 during morning rush hour, coinciding with the morning rush hour peak in NO_x concentrations. Unlike wintertime findings, summertime HO_2 concentrations in Tokyo were overestimated. An observed-to-modeled HO_2 ratio of 0.78 was reported. Trends

at high NO_x levels were not discussed as NO mixing ratios greater than 20 ppbv were not seen during this sampling period (Kanaya et al., 2007).

HO_2, HO_2NO_2, and hence the rate of ozone production may be underpredicted at high NO due to errors in calculated NO_x-dependent HO_x sources and sinks. We have investigated several possible sources of error. One possibility is an overestimate of the rate constant of R8, a sink of HO_x. The accepted rate constant for R8 has been subject to numerous revisions in the last decade (DeMore et al., 1997; Sander et al., 2000, 2003, 2006). Recent laboratory work at Jet Propulsion Laboratory and California Institute of Technology suggests that the 2000 JPL critical evaluation (Sander et al., 2000) may be closer than current recommendations (Sander et al., 2006) to the true rate (Okumura and Sander, 2005). The 2000 JPL critical evaluation recommended rate constant for R8 is approximately 30% lower for MILAGRO conditions than the most current evaluation. To test the importance of this on HO_2NO_2 levels, the recommended rate constant for R8 from the 2000 evaluation was substituted into the model. Figure 9 (top panel) illustrates the sensitivity of the modeled HO_2NO_2 mixing ratio to a change in the rate constant for R8. At high NO levels, use of the 2000 JPL recommended rate increases the mixing ratio of calculated HO_2NO_2, leading to better agreement between measured and calculated HO_2NO_2.

HO_2NO_2 mixing ratios and hence rate of ozone production may also be underpredicted at high NO_x due to missing calculated HO_x sources at high NO_x. Li et al. (2008) recently reported significant HO_x production from the reaction of excited-state NO_2 (NO_2^*) with H_2O:

$$NO_2^* + H_2O \rightarrow OH + HONO \quad \text{(R9)}$$

NO_2^* is formed through the excitation of NO_2 at wavelengths longer than 420 nm. These direct and indirect (via HONO photolysis) OH sources lead to increased concentrations of HO_x at elevated NO_x levels. Including this process in the box model, using the rate of R9 determined by Li et al. (2008), improves agreement with observed HO_2NO_2. As seen in Fig. 9 (middle panel), the inclusion of R9 increases the mixing ratio of calcu-

lated HO_2NO_2, again leading to better agreement between measured and calculated HO_2NO_2. Including both the reduced rate of R8 and the Li et al. (2008) process leads to increased levels of calculated HO_2NO_2 (Fig. 9, bottom panel). The transition to NO_x saturation appears to occur at higher NO_x levels than estimated by the NASA LaRC box model for Mexico City. This may have implications for engineering of improvements in air quality in the basin. If generally true, it suggests that further NO_x controls will yield reductions in smog levels. Significant uncertainties remain, however. It is unclear why the HO_x levels are generally underestimated. Although we identify several possible deficiencies in the photochemical mechanism that may contribute to an underprediction of HO_x, these are not sufficient to account for the discrepancy and each is uncertain and requires additional laboratory work to test these mechanisms (e.g., Wennberg and Dabdub, 2008). In addition, NO_x levels are generally much higher at the surface and so it is unclear if NO_x-limited conditions also apply.

Acknowledgements. The authors wish to thank C. M. Roehl for synthesizing the peroxynitric acid for calibration. P. Weibring and A. Fried, D. R. Blake, and R. E. Shetter provided formaldehyde, whole air sample, and solar actinic flux measurements, respectively, which provided constrains for the photochemical box model. The authors also wish to thank the C-130 crew and support team. The HO_2NO_2 measurements and their interpretation was made possible with the financial support of NASA (NAG: NNG06GB32B). J. D. C. acknowledges support from the EPA-STAR Fellowship Program (FP916334012). This work has not been formally reviewed by the EPA. The views expressed in this document are solely those of the authors and the EPA does not endorse any products or commercial services mentioned in this publication.

References

Amelynck, C., Schoon, N., and Arijs, E.: Gas phase reactions of CF_3O^- and $CF_3O^- \cdot H_2O$ with nitric, formic, and acetic acid, Int. J. Mass Spectrom., 203, 165–175, 2000. 2795, 2796

Amelynck, C., Van Bavel, A. M., Schoon, N., and Arijs, E.: Gas phase reactions of CF_3O^- and $CF_3O^- \cdot H_2O$ and their relevance to the detection of stratospheric HCl, Int. J. Mass Spectrom., 202, 207–216, 2000. 2795

Arnold, S. R., Chipperfield, M. P., and Blitz, M. A.: A three-dimensional model study of the effect of new temperature-dependent quantum yields for acetone photolysis, J. Geophys. Res.-Atmos., 110, D22305 doi:10.1029/2005JD005998, 2005. 2800

Atkinson, R., Baulch, D. L., Cox, R. A., Crowley, J. N., Hampson, R. F., Hynes, R. G., Jenkin, M. E., Rossi, M. J., and Troe, J.: Evaluated kinetic and photochemical data for atmospheric chemistry: Volume I – gas phase reactions of O_x, HO_x, NO_x and SO_x species, Atmos. Chem. Phys., 4, 1461–1738, 2004, http://www.atmos-chem-phys.net/4/1461/2004/. 2800

Barnes, I., Bastian, V., Becker, K. H., Fink, E. H., and Zabel, F.: Pressure-Dependence of the Reaction of OH with HO_2NO_2, Chem. Phys. Lett., 123, 28–32, 1986. 2794

Campos, T. L., Weinheimer, A. J., Zheng, J., Montzka, D. D., Walega, J. G., Grahek, F. E., Vay, S. A., Collins, J. E., Wade, L. O., Sachse, G. W., Anderson, B. E., Brune, W. H., Tan, D., Faloona, I., Baughcum, S. L., and Ridley, B. A.: Measurement of NO and NO_y emission indices during SUCCESS, Geophys. Res. Lett., 25, 1713–1716, 1998. 2795

Cantrell, C. A., Edwards, G. D., Stephens, S., Mauldin, L., Kosciuch, E., Zondlo, M., and Eisele, F.: Peroxy radical observations using chemical ionization mass spectrometry during TOPSE, J. Geophys. Res.-Atmos., 108, 8371, 2003. 2795

Crounse, J. D., McKinney, K. A., Kwan, A. J., and Wennberg, P. O.: Measurement of gas-phase hydroperoxides by chemical ionization mass spectrometry, Anal. Chem., 78, 6726–6732, 2006. 2795, 2796, 2798

DeMore, W. B., Sander, S. P., Golden, D. M., Hampson, R. F., Kurylo, M. J., Howard, C. J., Ravishankara, A. R., Kolb, C. E., and Molina, M. J.: Chemical Kinetics and Photochemical Data for Use in Stratospheric Modeling, Evaluation Number 12, JPL Publication 97-4, NASA Jet Propulsion Laboratory, California Institute of Technology, Pasadena, CA, USA, 1997. 2806

DuMouchel, W. H. and F. L. O'Brien: Integrating a Robust Option into a Multiple Regression Computing Environment, Computer Science and Statistics: Proceedings of the 21st Symposium on the Interface, Alexandria, VA, American Statistical Association, 1989. 2798, 2801

Emmerson, K. M., Carslaw, N., Carpenter, L. J., Heard, D. E., Lee, J. D., and Pilling, M. J.: Urban atmospheric chemistry during the PUMA campaign 1: Comparison of modelled OH and HO_2 concentrations with measurements, J. Atmos. Chem., 52, 143–164, 2005. 2804

Frost, G. J., Fried, A., Lee, Y. N., Wert, B., Henry, B., Drummond, J. R., Evans, M. J., Fehsenfeld, F. C., Goldan, P. D., Holloway, J. S., Hubler, G., Jakoubek, R., Jobson, B. T., Knapp, K.,

Kuster, W. C., Roberts, J., Rudolph, J., Ryerson, T. B., Stohl, A., Stroud, C., Sueper, D. T., Trainer, M., and Williams, J.: Comparisons of box model calculations and measurements of formaldehyde from the 1997 North Atlantic Regional Experiment, J. Geophys. Res.-Atmos., 107, 4060, doi:10.1029/2001JD000896, 2002. 2799

George, L. A., Hard, T. M., and O'Brien, R. J.: Measurement of free radicals OH and HO_2 in Los Angeles smog, J. Geophys. Res.-Atmos., 104, 11643–11655, 1999. 2805

Gierczak, T., Jimenez, E., Riffault, V., Burkholder, J. B., and Ravishankara, A. R.: Thermal Decomposition of HO_2NO_2 (Peroxynitric Acid, PNA): Rate Coefficient and Determination of the Enthalpy of Formation, J. Phys. Chem. A, 109, 586–596, 2005. 2794

Graham, R. A., Winer, A. M., and Pitts, J. N.: Temperature dependence of the unimolecular decomposition of pernitric acid and its atmospheric implications, Chem. Phys. Lett., 51, 215–220, 1977. 2794

Graham, R. A., Winer, A. M., and Pitts, J. N.: Pressure and Temperature-Dependence of Unimolecular Decomposition of HO_2NO_2, J. Chem. Phys., 68, 4505–4510, 1978. 2794

Heard, D. E., Carpenter, L. J., Creasey, D. J., Hopkins, J. R., Lee, J. D., Lewis, A. C., Pilling, M. J., Seakins, P. W., Carslaw, N., and Emmerson, K. M.: High levels of the hydroxyl radical in the winter urban troposphere, Geophys. Res. Lett., 31, L18112, doi:10.1029/2004GL020544, 2004. 2804, 2805

Huey, L. G., Hanson, D. R., and Howard, C. J.: Reactions of SF_6^- and I^- with atmospheric trace gases, J. Phys. Chem., 99, 5001–5008, 1995. 2797

Huey, L. G., Villalta, P. W., Dunlea, E. J., Hanson, D. R., and Howard, C. J.: Reactions of CF_3O^- with atmospheric trace gases, J. Phys. Chem., 100, 190–194, 1996. 2795, 2796

Jacob, D. J.: Introduction to Atmospheric Chemistry, Princeton University Press, 1999. 2802, 2803

Jaegle, L., Jacob, D. J., Brune, W. H., Faloona, I., Tan, D., Heikes, B. G., Kondo, Y., Sachse, G. W., Anderson, B., Gregory, G. L., Singh, H. B., Pueschel, R., Ferry, G., Blake, D. R., and Shetter, R. E.: Photochemistry of HO_x in the upper troposphere at northern midlatitudes, J. Geophys. Res.-Atmos., 105, 3877–3892, 2000. 2799

Jimenez, E., Gierczak, T., Stark, H., Burkholder, J. B., and Ravishankara, A. R.: Reaction of OH with HO_2NO_2 (Peroxynitric Acid): Rate Coefficients between 218 and 335 K and Product Yields at 298 K, J. Phys. Chem. A, 108, 1139–1149, 2004. 2794

Kanaya, Y., Cao, R. Q., Akimoto, H., Fukuda, M., Komazaki, Y., Yokouchi, Y., Koike, M., Tanimoto, H., Takegawa, N., and Kondo, Y.: Urban photochemistry in central Tokyo: 1. Observed

and modeled OH and HO_2 radical concentrations during the winter and summer of 2004, J. Geophys. Res.-Atmos., 112, D21312, doi:10.1029/2007JD008670, 2007. 2804, 2805, 2806

Kim, S., Huey, L. G., Stickel, R. E., Tanner, D. J., Crawford, J. H., Olson, J. R., Chen, G., Brune, W. H., Ren, X., Lesher, R., Wooldridge, P. J., Bertram, T. H., Perring, A., Cohen, R. C., Lefer, B. L., Shetter, R. E., Avery, M., Diskin, G., and Sokolik, I.: Measurement of HO_2NO_2 in the free troposphere during the intercontinental chemical transport experiment – North America 2004, J. Geophys. Res.-Atmos., 112, D12S01, doi:10.1029/2006JD007676, 2007. 2794, 2801, 2802

Knight, G., Ravishankara, A. R., and Burkholder, J. B.: UV absorption cross sections of HO_2NO_2 between 343 and 273 K, Phys. Chem. Chem. Phys., 4, 1432–1437, 2002. 2794

Li, S. P., Matthews, J., and Sinha, A.: Atmospheric hydroxyl radical production from electronically excited NO_2 and H_2O, Science, 319, 1657–1660, 2008. 2806, 2807

Lurmann, F. W., Lloyd, A. C., and Atkinson, R.: A Chemical Mechanism for Use in Long-Range Transport Acid Deposition Computer Modeling, J. Geophys. Res.-Atmos., 91, 905–936, 1986. 2800

Macleod, H., Smith, G. P., and Golden, D. M.: Photodissociation of Pernitric Acid (HO_2NO_2) at 248 nm, J. Geophys. Res.-Atmos., 93, 3813–3823, 1988. 2794

Madronich, S. and Flocke, S.: The role of solar radiation in atmospheric chemistry, in: Handbook of Environmental Chemistry, edited by: Boule, P., Springer, 1–26, 1998. 2800

Martinez, M., Harder, H., Kovacs, T. A., Simpas, J. B., Bassis, J., Lesher, R., Brune, W. H., Frost, G. J., Williams, E. J., Stroud, C. A., Jobson, B. T., Roberts, J. M., Hall, S. R., Shetter, R. E., Wert, B., Fried, A., Alicke, B., Stutz, J., Young, V. L., White, A. B., and Zamora, R. J.: OH and HO_2 concentrations, sources, and loss rates during the Southern Oxidants Study in Nashville, Tennessee, Summer 1999, J. Geophys. Res.-Atmos., 108, D194617, doi:10.1029/2003JD003551, 2003. 2804

Murphy, J. G., Thornton, J. A., Wooldridge, P. J., Day, D. A., Rosen, R. S., Cantrell, C., Shetter, R. E., Lefer, B., and Cohen, R. C.: Measurements of the sum of HO_2NO_2 and $CH_3O_2NO_2$ in the remote troposphere, Atmos. Chem. Phys., 4, 377–384, 2004, http://www.atmos-chem-phys.net/4/377/2004/. 2793, 2794, 2802

Niki, H., Maker, P. D., Savage, C. M., and Breitenbach, L. P.: Fourier transform IR spectroscopic observation of pernitric acid formed via $HOO + NO_2 \rightarrow HOONO_2$, Chem. Phys. Lett., 45, 564–566, 1977. 2793

Olson, J. R., Crawford, J. H., Chen, G., Fried, A., Evans, M. J., Jordan, C. E., Sandholm, S. T.,

Davis, D. D., Anderson, B. E., Avery, M. A., Barrick, J. D., Blake, D. R., Brune, W. H., Eisele, F. L., Flocke, F., Harder, H., Jacob, D. J., Kondo, Y., Lefer, B. L., Martinez, M., Mauldin, R. L., Sachse, G. W., Shetter, R. E., Singh, H. B., Talbot, R. W., and Tan, D.: Testing fast photochemical theory during TRACE-P based on measurements of OH, HO_2, and CH_2O, J. Geophys. Res.-Atmos., 109, D15S10, doi:10.1029/2003JD004278, 2004. 2799

Olson, J. R., Crawford, J. H., Chen, G., Brune, W. H., Faloona, I. C., Tan, D., Harder, H., and Martinez, M.: A reevaluation of airborne HO_x observations from NASA field campaigns, J. Geophys. Res.-Atmos., 111, D10301, doi:10.1029/2005JD006617, 2006. 2799

Okumura, M. and Sander, S. P: Gas-Phase Formation Rates of Nitric Acid and its Isomers under Urban Conditions, State of California Air Resources Board, 2005. 2806

Ravishankara, A. R., Dunlea, E. J., Blitz, M. A., Dillon, T. J., Heard, D. E., Pilling, M. J., Strekowski, R. S., Nicovich, J. M., and Wine, P. H.: Redetermination of the rate coefficient for the reaction of $O(^1D)$ with N_2, Geophys. Res. Lett., 29, 1745, doi:10.1029/2002GL014850, 2002. 2800

Ren, X. R., Harder, H., Martinez, M., Lesher, R. L., Oliger, A., Simpas, J. B., Brune, W. H., Schwab, J. J., Demerjian, K. L., He, Y., Zhou, X. L., and Gao, H. G.: OH and HO_2 chemistry in the urban atmosphere of New York City, Atmos. Environ., 37, 3639–3651, 2003. 2804, 2805

Ren, X. R., Brune, W. H., Mao, J. Q., Mitchell, M. J., Lesher, R. L., Simpas, J. B., Metcalf, A. R., Schwab, J. J., Cai, C. X., Li, Y. Q., Demerjian, K. L., Felton, H. D., Boynton, G., Adams, A., Perry, J., He, Y., Zhou, X. L., and Hou, J.: Behavior of OH and HO_2 in the winter atmosphere in New York City, Atmos. Environ., 40, S252–S263, 2006. 2804

Roehl, C. M., Nizkorodov, S. A., Zhang, H., Blake, G. A., and Wennberg, P. O.: Photodissociation of Peroxynitric Acid in the Near-IR, J. Phys. Chem. A, 106, 3766–3772, 2002. 2794, 2797, 2800

Rothman, L. S., Jacquemart, D., Barbe, A., Benner, D. C., Birk, M., Brown, L. R., Carleer, M. R., Chackerian, C., Chance, K., Coudert, L. H., Dana, V., Devi, V. M., Flaud, J. M., Gamache, R. R., Goldman, A., Hartmann, J. M., Jucks, K. W., Maki, A. G., Mandin, J. Y., Massie, S. T., Orphal, J., Perrin, A., Rinsland, C. P., Smith, M. A. H., Tennyson, J., Tolchenov, R. N., Toth, R. A., Vander Auwera, J., Varanasi, P., and Wagner, G.: The HITRAN 2004 molecular spectroscopic database, J. Quant. Spectrosc. Ra., 96, 139–204, 2005. 2796, 2797

Sander, S. P., Friedl, R. R., DeMore, W. B., Golden, D. M., Kurylo, M. J., Hampson, R. F., Huie, R. E., Moortgat, G. K., Ravishankara, A. R., Kolb, C. E., and Molina, M. J.: Chemical Kinetics

and Photochemical Data for Use in Stratospheric Modeling Supplement to Evaluation 12: Update of Key Reactions, JPL Publication 00-3, NASA Jet Propulsion Laboratory, California Institute of Technology, Pasadena, CA, USA, 2000. 2806

Sander, S. P., Friedl, R. R., DeMore, W. B., Golden, D. M., Kurylo, M. J., Huie, R. E., Orkin, V. L., Moortgat, G. K., Ravishankara, A. R., Kolb, C. E., and Molina, M. J., and Finlayson-Pitts, B. J.: Chemical Kinetics and Photochemical Data for Use in Atmospheric Studies, Evaluation Number 14 JPL Publication 02-25, NASA Jet Propulsion Laboratory, California Institute of Technology, Pasadena, CA, USA, 2003. 2800, 2806

Sander, S. P., Friedl, R. R., Golden, D. M., Kurylo, M. J., Moortgat, G. K., Keller-Rudek, H., Wine, P. H., Ravishankara, A. R., Kolb, C. E., Molina, M. J., Finlayson-Pitts, B. J., Huie, R. E., and Orkin, V. L.: Chemical Kinetics and Photochemical Data for Use in Atmospheric Studies, Evaluation Number 15 JPL Publication 06-2, NASA Jet Propulsion Laboratory, California Institute of Technology, Pasadena, CA, USA, 2006. 2806

Seinfeld, J. H., and Spryros N. Pandis: Atmospheric Chemistry and Physics, 2nd ed., John Wiley & Sons, Inc., 2006. 2793, 2802, 2804

Shetter, R. E. and Muller, M.: Photolysis frequency measurements using actinic flux spectroradiometry during the PEM-Tropics mission: Instrumentation description and some results, J. Geophys. Res.-Atmos., 104, 5647–5661, 1999. 2800

Shirley, T. R., Brune, W. H., Ren, X., Mao, J., Lesher, R., Cardenas, B., Volkamer, R., Molina, L. T., Molina, M. J., Lamb, B., Velasco, E., Jobson, T., and Alexander, M.: Atmospheric oxidation in the Mexico City Metropolitan Area (MCMA) during April 2003, Atmos. Chem. Phys., 6, 2753–2765, 2006, http://www.atmos-chem-phys.net/6/2753/2006/. 2805

Slusher, D. L., Pitteri, S. J., Haman, B. J., Tanner, D. J., and Huey, L. G.: A chemical ionization technique for measurement of pernitric acid in the upper troposphere and the polar boundary layer, Geophys. Res. Lett., 28, 3875–3878, 2001. 2794

Smith, C. A., Molina, L. T., Lamb, J. J., and Molina, M. J.: Kinetics of the Reaction of OH with Pernitric and Nitric-Acids, Int. J. Chem. Kinet., 16, 41–55, 1984. 2794

Street, J. O., Carroll, R. J., and Ruppert, D.: A Note on Computing Robust Regression Estimates via Iteratively Reweighted Least Squares, The American Statistician, 42, 152–154, 1988. 2798, 2801

Trevor, P. L., Black, G., and Barker, J. R.: Reaction-Rate Constant for OH + $HOONO_2$ → Products over the Temperature-Range 246 to 324 K, J. Phys. Chem., 86, 1661–1669, 1982. 2794

Weinheimer, A. J., Montzka, D. D., Campos, T. L., Walega, J. G., Ridley, B. A., Donnelly, S. G., Keim, E. R., Del Negro, L. A., Proffitt, M. H., Margitan, J. J., Boering, K. A., Andrews, A. E., Daube, B. C., Wofsy, S. C., Anderson, B. E., Collins, J. E., Sachse, G. W., Vay, S. A., Elkins, J. W., Wamsley, P. R., Atlas, E. L., Flocke, F., Schauffler, S., Webster, C. R., May, R. D., Loewenstein, M., Podolske, J. R., Bui, T. P., Chan, K. R., Bowen, S. W., Schoeberl, M. R., Lait, L. R., and Newman, P. A.: Comparison between DC-8 and ER-2 species measurements in the tropical middle troposphere: NO, NO_y, O_3, CO_2, CH_4, and N_2O, J. Geophys. Res.-Atmos., 103, 22087–22096, 1998. 2795

Wennberg, P. O. and Dabdub, D.: Atmospheric chemistry – Rethinking ozone production, Science, 319, 1624–1625, 2008. 2807

Zabel, F.: Unimolecular Decomposition of Peroxynitrates, Z. Phys. Chem., 188, 119–142, 1995. 2794

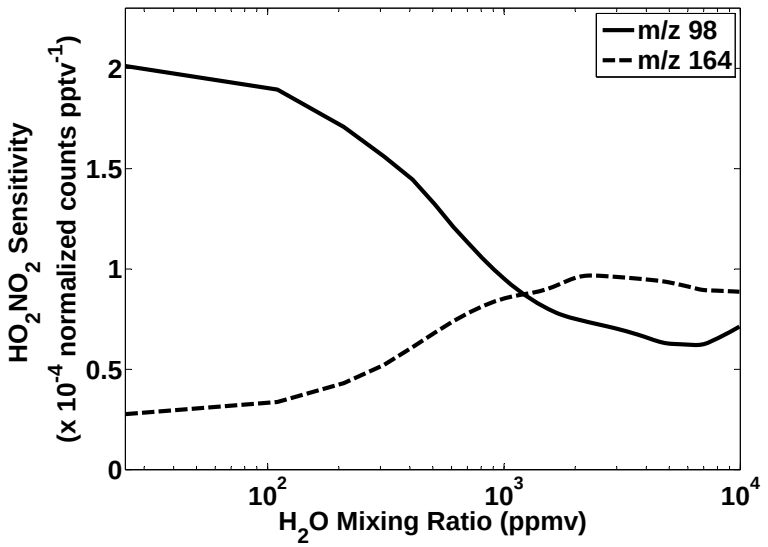

Fig. 1. Sensitivity curves for *m/z* 98 (solid) and *m/z* 164 (dash) as a function of H_2O mixing ratio in the flow tube. The sensitivity curves are used to calculate the final mixing ratios of HO_2NO_2.

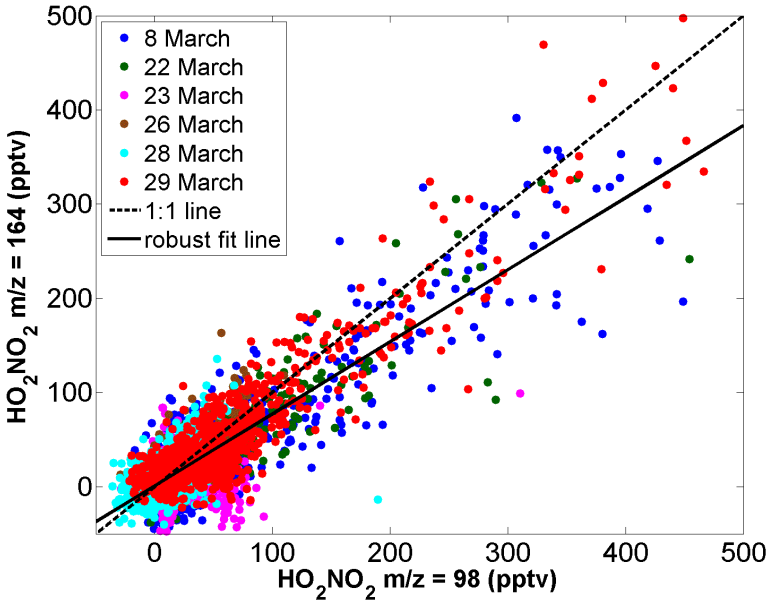

Fig. 2. HO_2NO_2 is measured with two ions: products of fluoride transfer (*m/z*=98) and clustering (*m/z*=164). The data are colored by flight date. The data shown are observations obtained when the measured NO_y differs by less than 10% between *m/z* 98 and *m/z* 164 sampling times. The slope of the robust fit line is 0.90; the intercept is 0.76 pptv; R^2=0.94. Independent measurements of HO_2NO_2 from these two ions agree very well, indicating that these masses are selective to HO_2NO_2.

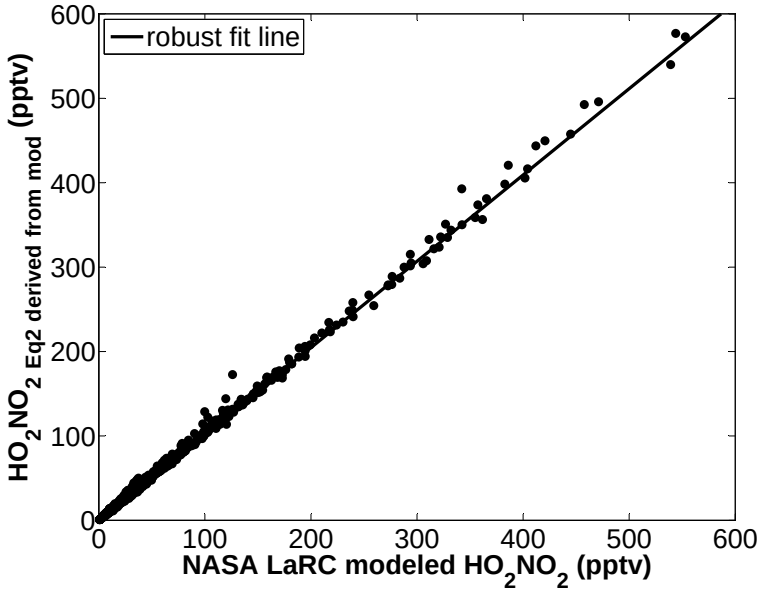

Fig. 3. $[HO_2NO_2]_{ss}$, calculated from Eq. (2), using modeled values of HO_2 and NO_2 versus HO_2NO_2 predicted by the NASA LaRC box model. The slope of the robust fit line is 1.02; intercept is 0.10 pptv; R^2=0.99, demonstrating that Eq. (2) is a valid simplification under MILAGRO conditions.

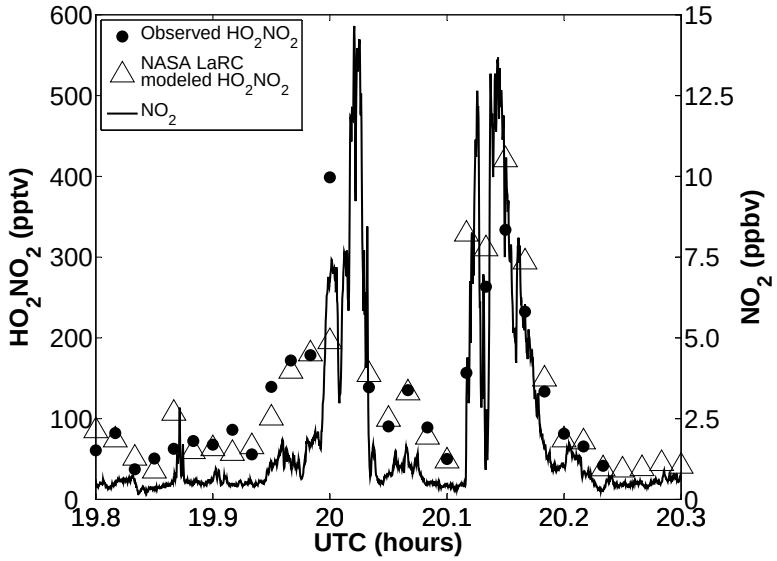

Fig. 4. Mixing ratios of HO_2NO_2 and NO_2 during Flight 29 March 2006 in an air mass heavily impacted by pollution. Dots are CIMS measurements of HO_2NO_2. Triangles are NASA LaRC box model values of HO_2NO_2. The solid line is observed NO_2 mixing ratio. Variations in the observed and modeled HO_2NO_2 mixing ratios closely follow variations in NO_2.

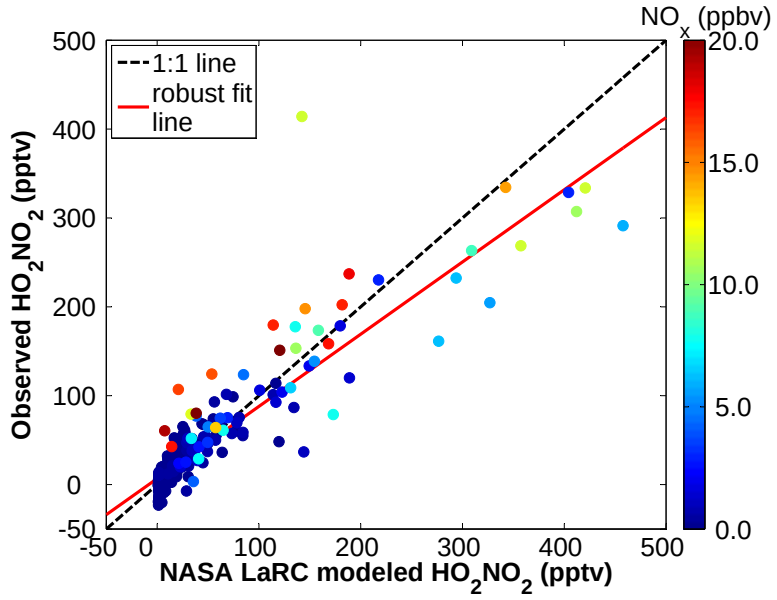

Fig. 5. Observed HO_2NO_2 versus NASA LaRC box model values of HO_2NO_2. The data presented are observed and modeled values at times when the model was constrained by NMHC observations. The slope of the robust fit line is 0.81; intercept is 6.74 pptv; R^2=0.82.

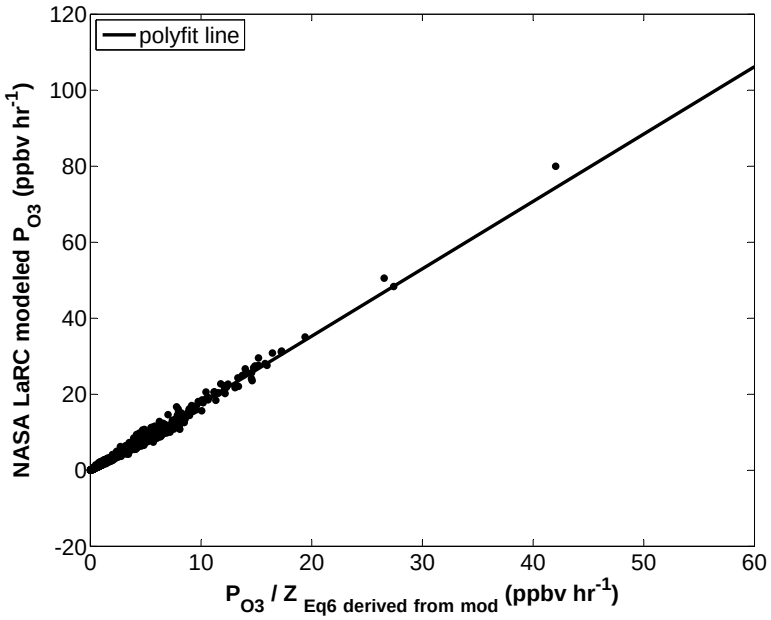

Fig. 6. The rate of production of ozone calculated using Eq. (6) and modeled values of HO_2NO_2, NO, and NO_2 is compared to the ozone production rate predicted by the NASA LaRC box model.

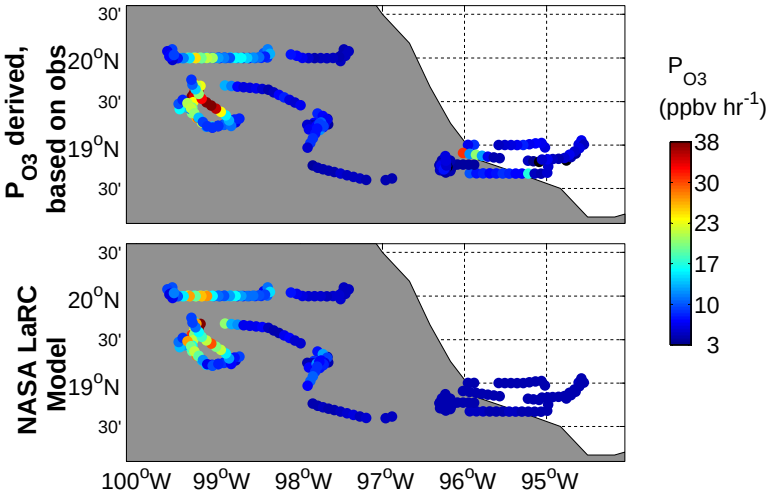

Fig. 7. Rate of ozone production along the flight track of 29 March 2006. Top panel is the rate calculated using observed values of HO_2NO_2, NO, and NO_2 and Eq. (6). Bottom panel is the rate predicted by the NASA LaRC box model.

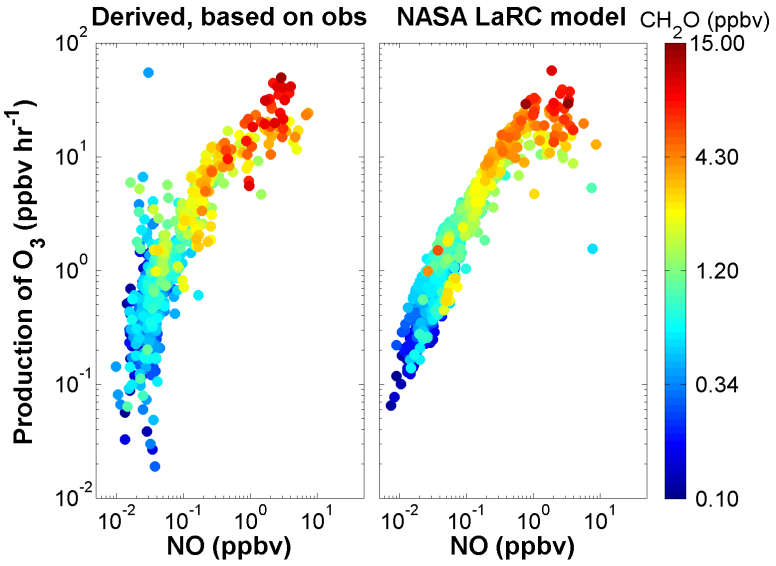

Fig. 8. Rate of ozone production versus mixing ratio of NO colored by the mixing ratio of formaldehyde. P_{O_3} derived from Eq. (6), based on measurements of HO_2NO_2 and NO_x are shown in the left panel. NASA LaRC box model predictions of P_{O_3} are shown in the right panel.

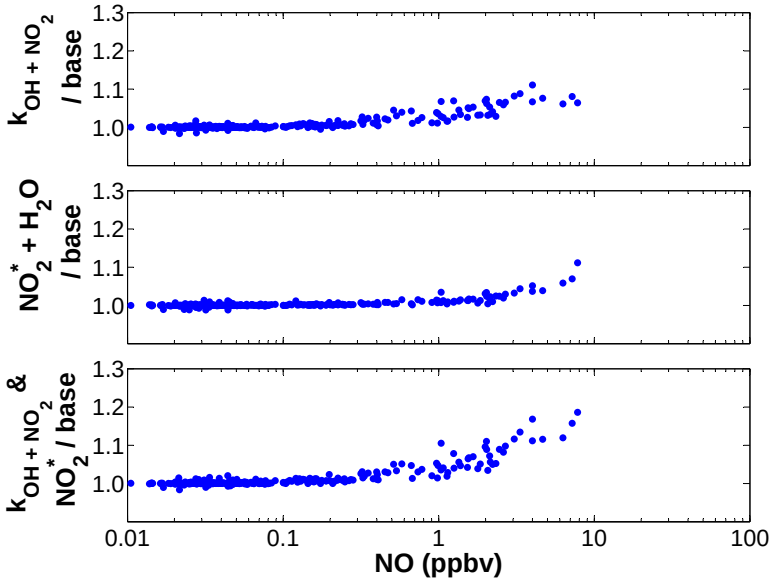

Fig. 9. Three different variations of the base model were investigated. Model variations are divided by the base model and plotted versus NO. Use of the 2000 JPL recommendation for the rate constant for $OH+NO_2$ and inclusion of the $NO_2^*+H_2O$ reaction result in higher HO_2NO_2 mixing ratios than estimated by the base model. This leads to better agreement between measured and calculated HO_2NO_2.